Precision Mechanics & Digital Fabrication
https://www.acadlore.com/journals/PMDF

Analysis and Experimental Study of the Composite Mechanical Bulging Process for Medium-Duty Commercial Vehicle Drive Axle Housing

Pan Li [1*], Jitao Zhou[1], Xuexu Yuan[1], Junwei Zhao[1*], Xiaowei Fu[1], Jian Zeng[2]

[1] School of Emergency Equipment, North China Institute of Science and Technology, 065201 Langfang, China
[2] School of Materials Science and Engineering, Shanghai Jiao Tong University, 200240 Shanghai, China

[*] Correspondence: Pan Li (lipanzy@ncist.edu.cn); Junwei Zhao (shower@yeah.net)

Received: 11-08-2024 **Revised:** 12-20-2024 **Accepted:** 12-26-2024

Citation: P. Li, J. T. Zhou, X. X. Yuan, J. W. Zhao, X. W. Fu, and J. Zeng, "Analysis and experimental study of the composite mechanical bulging process for medium-duty commercial vehicle drive axle housing," *Precis. Mech. Digit. Fabr.*, vol. 1, no. 4, pp. 235–251, 2024. https://doi.org/10.56578/pmdf010405.

Abstract: A novel composite mechanical bulging process suitable for the manufacture of medium-duty commercial vehicle drive axle housings is proposed. The analytical expression for the limit bulging forming coefficient of tube blanks under conditions below the metal recrystallization temperature is derived, and the influence of the matching of various force parameters on the limit bulging forming coefficient is analyzed. The appropriate range for the axial auxiliary load during radial bulging is also presented. Based on the derived theory, a 5-ton commercial vehicle drive axle housing is selected as the research object. The key processes in the forming process are numerically simulated to obtain the metal flow state, stress-strain distribution, and wall thickness variation. The types and locations of defects that may occur during the bulging process are also predicted. To address the phenomenon of local wall thinning in the composite mechanical bulging process of the drive axle housing, a set of orthogonal simulation experiments is designed, focusing on the wall thickness thinning rate in the bridge arch bulging area and the crack-prone region, with respect to the process parameters. Based on the numerical simulation results, response surface equations are established for the expansion core's movement speed and axial auxiliary thrust in relation to the wall thickness thinning rate. Through parameter estimation of the response surface equation and regression analysis of significant influencing factors, the effects of process parameters on wall thickness thinning are obtained: the thinning rate in the bridge arch bulging area decreases with increasing expansion core movement speed and axial auxiliary thrust, while the thinning rate in the crack-prone region increases. The optimization of the response surface model and the determination of the optimal process parameter combination, based on field production conditions, show that the numerical simulation results and the wall thickness measurements from process experiments are in close agreement. No cracks occur in the axle housing, and the thinning is effectively alleviated. In contrast, mechanical bulging without axial auxiliary thrust leads to cracks, thus validating the feasibility of the proposed process scheme and the effectiveness of the parameter optimization. This research provides valuable technical reference for upgrading the manufacturing technology of large-span axle-tube products.

Keywords: Drive axle housing; Composite mechanical bulging; Bulging coefficient; Numerical simulation; Response surface method; Multi-objective optimization

1 Introduction

The drive axle is a key component of the chassis driving system for rear-wheel-drive commercial vehicles. In addition to bearing the weight of the vehicle body, it also plays a role in transmitting the vehicle's driving power, as well as in deceleration and differential functions [1–3]. The drive axle housing, as the supporting body for the drive axle's reducer, differential, and half shafts, is also connected to the rear wheels and the drive shaft at both ends and in the middle. During the operation of commercial vehicles, the drive axle housing continuously bears road reaction forces, torque, and various vibrations and impacts transmitted by the wheels. It is the core load-bearing part that ensures the proper functioning of the drive axle, and its quality largely determines the service life and driving safety of commercial vehicles [4–6]. However, the drive axle housing is a large-span, irregularly shaped, hollow shaft component with a complex shape and large mass, making its production and manufacturing extremely challenging. Currently, the mainstream drive axle housing products in the market are mostly produced using traditional casting

and stamping-welding processes [7, 8]. Since the global economy has entered a new normal of slow development, the contradiction between overcapacity in the production of drive axle housing products in the main manufacturing countries and insufficient market demand has become increasingly prominent. The product structure and production processes urgently need to be adjusted and upgraded. This is mainly reflected in: casting-type axle housings being assembled from a cast axle housing body and forged half-shaft sleeves, resulting in large volume and weight, complex manufacturing processes, low yield, high material consumption, and long production cycles. These products cannot meet the lightweight requirements of automotive components, resulting in low market demand and production volume, with such housings primarily used in heavy-duty special vehicles; stamping-welded drive axle housings are made from steel plates, which are stamped into half-shells and then welded together. Afterward, the axle housing rear cover, reinforcement rings, axle heads, and spring seats are welded onto the housing to form the complete axle housing. Since the various parts of the stamped-welded axle housing are joined through welding processes, the presence of weld seams significantly limits the strength and rigidity of these housings. After long-term use, issues such as oil leakage and local fractures often arise, making them unsuitable for the development needs of heavy-duty commercial vehicles [9–14]. Furthermore, these traditional axle housing products have limitations in terms of performance, service life, and production line integration, which also restrict the implementation of energy-saving and emission-reduction policies in vehicle manufacturing [15, 16]. In recent years, as countries worldwide have placed increasing emphasis on vehicle lightweighting and green manufacturing, the concept of integrated structural design for automotive components, which balances lightness and safety, has been continuously deepened in the automotive manufacturing field. Meanwhile, domestic and international vehicle axle manufacturers have begun designing the next generation of commercial vehicle drive axles, and the manufacturing technology for drive axle housings has rapidly shifted from traditional overall casting and stamping-welding processes toward seamless steel tube integrated plastic forming, aiming to eliminate weld seams, reduce weight, and improve performance and service life [17–19]. New integrated drive axle housings have higher safety and reliability, meeting the development trend of lightweight vehicle structures, and will inevitably become the mainstream product to replace cast and welded axle housings. The development of the forming process has therefore become a research hotspot in the vehicle manufacturing industry, with the difficulty of achieving this technological concept lying in the expansion forming of the bridge arch section of the drive axle housing using seamless steel pipes as the raw material [20–23]. Although many scholars have proposed various methods for expanding the bridge arch of thick-walled drive axle housings and conducted a series of studies, the high cost of sample production, the lack of specialized power equipment, and the absence of matching automatic process transfer devices have led most research to focus on theoretical studies and numerical simulations, without forming a mature expansion forming process for drive axle housings. Few experimental verifications and pilot productions are publicly available.

This paper focuses on the integrated manufacturing of drive axle housings and, based on the structural characteristics of the drive axle housing, proposes a new forming process using seamless steel pipes for mechanical expansion forming under the condition of axial auxiliary thrust. The process flow of the proposed composite mechanical expansion forming technology for drive axle housings is detailed. The analytical expression for the pipe billet expansion forming coefficient under this process is derived, and the influence of the matching relationship between the force parameters in different directions during the forming process on the forming coefficient is studied. Combining a certain model of commercial vehicle drive axle housing, numerical simulations, and process experiments are carried out to explore the optimization of the bridge arch forming process for medium-sized commercial vehicle drive axle housings. The response surface equation is established to explore the influence of key process parameters on the optimization objectives. The optimization targets include alleviating the thinning of the bridge arch wall and effectively preventing the tearing of the sidewalls at both ends of the preformed holes. The results of numerical simulations and process experiments are compared and analyzed, and the proposed forming process is analyzed and verified. Compared with traditional drive axle housing manufacturing technologies, the composite expansion forming technology proposed in this paper can promote the production mode of large, complex shaft-tube components from dispersed assembly to integrated manufacturing. It can greatly avoid the impact of weld seams on the performance of the axle housing, significantly improve the load-bearing capacity of the axle housing, and simplify the production process. While saving resources and reducing production costs, it significantly increases the service life of the axle housing. It also contributes to achieving overall heat treatment of the axle housing to strictly control product quality, thus providing an important reference for the innovation and breakthrough of commercial vehicle drive axle housing manufacturing technology.

2 Composite Mechanical Expansion Forming Process for Drive Axle Housing

The composite mechanical expansion forming process for the drive axle housing proposed in this paper uses square steel tubes as raw materials to complete the formation of the bridge arch. The detailed process flow is shown in Figure 1. Before the composite mechanical expansion of the bridge arch, two pre-set shaped through-holes need to be cut on the mutually parallel side surfaces of the tube billet in the middle section. Then, pre-expansion tapered

mandrels are used to blind-punch the preformed through-holes, causing the two sides of the bridge arch to expand and form a space for accommodating the expansion mandrels. The composite mechanical expansion process, i.e., the inward radial expansion process of the bridge arch, involves using a braking device to drive the two expansion mandrels to move in the opposite direction along the radius of the bridge arch, while applying equal axial auxiliary thrusts to both ends of the tube billet. This causes the bridge arch section to expand to the required maximum radial size, thereby forming the curved hole. The role of the applied auxiliary thrust is to effectively alleviate stress concentration in the expansion area of the tube billet, preventing local tearing in the expansion zone while mainly focusing on radial expansion using the expansion mandrel. After the radial expansion is complete, the tube section containing the curved hole is heated to the recrystallization temperature of the steel tube material. The outward wall of the expansion area is then fully conformed to the mold through reverse reshaping by the radial and axial mandrels, thus achieving precise forming of the shape and dimensions.

Unlike the mechanical expansion forming of heavy-duty commercial vehicle drive axle housings, the wall thickness of medium-sized vehicle drive axle housings is smaller. Therefore, prior to composite mechanical expansion, there is no need to preheat the expansion zone to high temperatures. The complete forming of the bridge arch is achieved through the reshaping phase after preheating, and no axial auxiliary thrust needs to be applied during the reshaping phase. It should be noted that the wall thickness distribution of the drive axle housing expansion zone has already formed during the composite mechanical expansion phase, and the impact of the internal reshaping mandrel's compaction on the wall thickness distribution during the reshaping phase is minimal. Therefore, for medium-sized commercial vehicle drive axle housings, the composite mechanical expansion process remains the core stage of bridge arch forming.

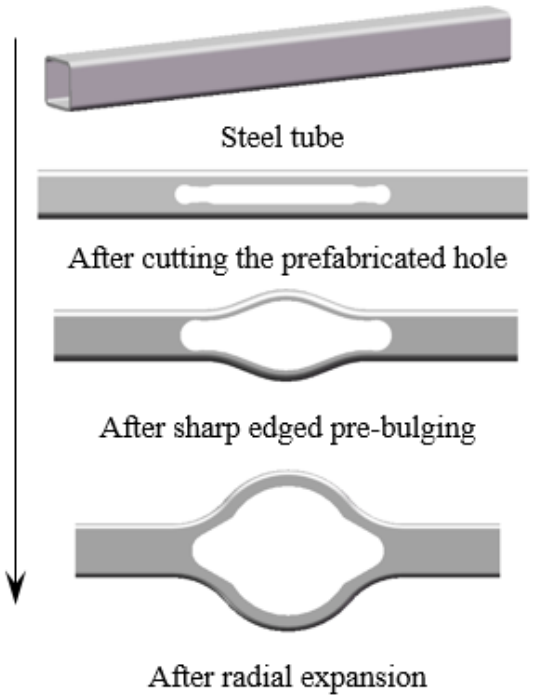

Figure 1. Main process flow diagram of composite mechanical expansion forming for drive axle housing

3 Mechanical Expansion Forming Coefficient of Square Steel Tubes

The ultimate expansion forming coefficient of the tube billet characterizes the maximum degree to which the expansion region of the square tube can be expanded under corresponding loading conditions and external environments. It is crucial for guiding the development of forming procedures. For tube billets with relatively large wall thickness, the central part of the steel tube needs to be heated to a temperature above the material's recrystallization temperature before expansion. Existing research literature has indicated that under high-temperature conditions, the ultimate expansion ratio of metallic tubes should not exceed 2.5 [22]. For medium wall thickness or lower expansion degrees in the axle housing, expansion can be performed at room temperature or heated to below the material's recrystallization temperature to meet the expansion requirements. However, there are no clear research results on determining the mechanical expansion forming coefficient of tube billets below the recrystallization temperature.

This paper focuses on the metal's stress and strain during the composite mechanical expansion forming of the bridge arch, combining the conditions of metal plastic deformation and the material's constitutive equation, and derives the expression for the ultimate forming coefficient of the tube billet composite mechanical expansion under conditions where deformation may cause work hardening, i.e., below the recrystallization temperature.

The analysis of a unit body extracted from the inner wall deformation zone of the steel tube's middle section is shown in Figure 2. Since the tube billet's middle section is interrupted by preformed holes, the stress in the direction perpendicular to the plane of the figure can be neglected. Therefore, the stress distribution in the unit body consists of hoop stress σ_θ and radial stress σ_ρ, which can be approximated as a plane stress state. Thus, its plasticity condition is:

$$\sigma_\theta^2 - \sigma_\theta \sigma_p + \sigma_\rho^2 = \sigma_s^2 \tag{1}$$

According to the stress equilibrium condition, we obtain:

$$\sigma_\rho \cdot R_\rho - \sigma_\theta \cdot f = 0 \tag{2}$$

In this equation, R_ρ is the curvature radius of the inner edge of the bridge arch, f is the wall thickness at this location of the bridge housing, and σ_s is the yield stress of the material.

Most engineering metals, when undergoing large deformations below the recrystallization temperature, experience work hardening, and their true stress-strain curve approximates a parabolic shape. The true stress-strain curve of the material can be precisely expressed in a power law form [23]:

$$\sigma_s = B \in^n \tag{3}$$

From the empirical equation of the parabolic true stress-strain curve, the constants B and n can be obtained as:

$$n = \epsilon_b = \ln(1 + \delta_u); B = Y_b / \epsilon_b^{\epsilon_b}; Y_b = \sigma_b (1 + \delta_u)$$

Thus:

$$\sigma_s = \sigma_b \frac{\epsilon^n}{n^n} \tag{4}$$

where, δ_u is the tensile strain of the material, and Y_b and ϵ_b are the equivalent stress and logarithmic strain at the instability point on the stress-strain curve, respectively.

Assuming that volume remains constant during plastic deformation, let ξ=$\varepsilon_\rho / \varepsilon_\theta$, introducing the equivalent strain equation [24], we get:

$$\epsilon = \frac{2}{\sqrt{3}} \sqrt{1 + \xi + \xi^2} \cdot \epsilon_\theta \tag{5}$$

Let the outer diameter of the bridge arch after expansion be D_t, and the outer diameter before expansion be D_{t-1}. For the material point at the maximum expansion position, we have:

$$\epsilon_\theta = \ln(D_t / D_{t-1}) \tag{6}$$

Assuming that during radial mechanical expansion, the plastic strain and stress offset of the material point at the maximum expansion position of the bridge housing are proportional, we get:

$$\xi = \frac{\epsilon_\rho}{\epsilon_\theta} = \frac{\sigma'_\rho}{\sigma'_\theta} = \frac{\sigma_\rho - \sigma_\mathrm{m}}{\sigma_\theta - \sigma_\mathrm{m}} = \frac{2\sigma_\rho - \sigma_\theta}{2\sigma_\theta - \sigma_\rho} \tag{7}$$

It can be derived as:

$$\frac{\sigma_\theta}{\sigma_\theta} = \frac{2\xi + 1}{2 + \xi} \tag{8}$$

Substituting Eq. (8) into Eq. (4), we get:

$$\sigma_\theta^2 \left[1 - \frac{\sigma_\rho}{\sigma_\theta} + \left(\frac{\sigma_\rho}{\sigma_\theta} \right)^2 \right] = \sigma_s^2$$

That is:

$$\sqrt{1 - \frac{2\xi + 1}{2 + \xi} + \left(\frac{2\xi + 1}{2 + \xi} \right)^2} \cdot \sigma_\theta = Y_b \cdot \left(\frac{\frac{2}{\sqrt{3}} \sqrt{1 + \xi + \xi^2}}{n} \right)^n \left(\ln \frac{D_t}{D_{t-1}} \right)^n \tag{9}$$

Since $\sigma_\theta \leq Y_b$, the ultimate expansion coefficient K can be expressed as:

$$K=\frac{D_t}{D_{t-1}} \leq e^{\frac{\sqrt{3}\sqrt[n]{\left(1-\frac{2\xi+1}{2+\xi}+\left(\frac{2\xi+1}{2+\xi}\right)^2\right)^{\frac{1}{2}}}}{2\sqrt{1+\xi+\xi^2}}\cdot n} \tag{10}$$

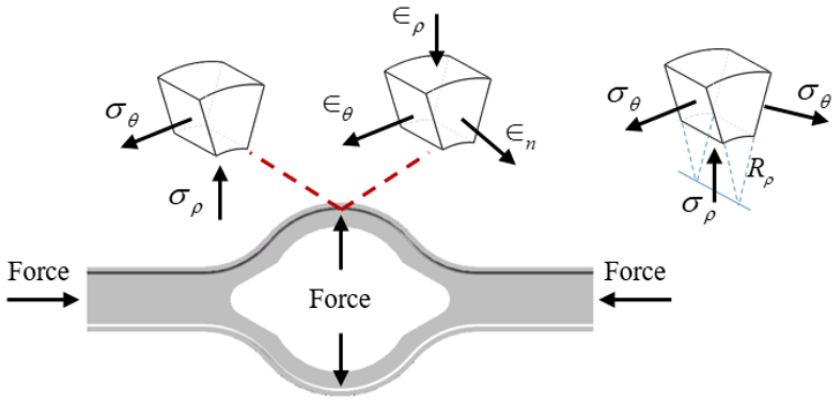

Figure 2. Schematic diagram of the extracted unit body and its stress state analysis

4 Force Matching in Composite Mechanical Expansion Forming

According to the forming principles of the process, the forming of the bridge housing occurs in the tube segment that includes the preformed hole in the middle section of the steel tube raw material, while the straight arm sections at both ends of the steel tube do not undergo plastic deformation. Therefore, the compressive stress on both ends of the steel tube must not exceed the true yield stress of the material at room temperature. If required, the expansion zone can be heated to a certain temperature before expansion, but below the material's recrystallization temperature. Additionally, the deformation heat generated during the metal's deformation process means that, whether heated or not, the temperature of the metal in the middle section of the tube billet will always be higher than that of the straight arm sections that do not participate in the expansion. Due to the effect of temperature, the yield stress of the metal in the expansion zone is much lower than that of the metal in the straight arm sections. Therefore, the value of the auxiliary thrust at both ends of the bridge housing during expansion can be determined: the absolute value of the compressive stress generated by the auxiliary thrust on the expansion section at the maximum expansion position of the bridge arch must not exceed the true yield stress of the metal material at that temperature.

The axial auxiliary thrust is set as T. When the pipe blank expansion area is below the recrystallization temperature of the metal, the maximum hoop stress σ_θ of the material point at the maximum expansion location can be expressed as:

$$\sigma_\theta = T/2S + \sigma_s \tag{11}$$

Let the expansion mandrel surface area be S_0, and the single-side expansion load be F_b, then the radial stress σ_ρ during expansion can be expressed as:

$$\sigma_\rho = F_b/S_0 \tag{12}$$

In the above equation, σ_s is the true yield stress of the bridge housing metal at the corresponding temperature, and the absolute value of $F_p/2S$ and σ_ρ must be less than σ_s, where S is the area of a single crosssection at the maximum expansion position and remains approximately unchanged during expansion.

In the composite mechanical expansion forming process, the stress-strain states of the various points in the expansion zone are different. For most of the forming stage, the stress and strain states at the maximum expansion position of the bridge arch constrain the limit expansion amount of the expansion deformation. Therefore, by adjusting the auxiliary thrust and expansion force, and controlling the stress-strain state at the material point at the maximum expansion position, it is possible to regulate the limit expansion forming coefficient. From Eqs. (7), (8), and (10), the effects of the changes in $\sigma_\rho/\sigma_\theta$ and $\varepsilon_\rho/\varepsilon_\theta$ on the limit expansion forming coefficient during expansion below the recrystallization temperature can be obtained, as shown in Figure 3 and Figure 4. From the figures, it can be seen that, under the condition that the metal in the expansion zone is not torn, the higher the absolute value of the ratio of radial expansion stress to hoop stress and the ratio of radial strain to hoop strain, the higher the limit expansion forming coefficient.

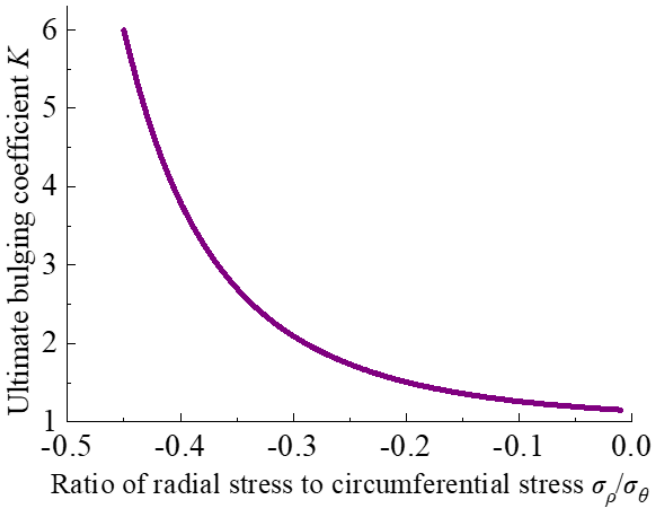

Figure 3. Effect of $\sigma_\rho/\sigma_\theta$ on the limit expansion forming coefficient

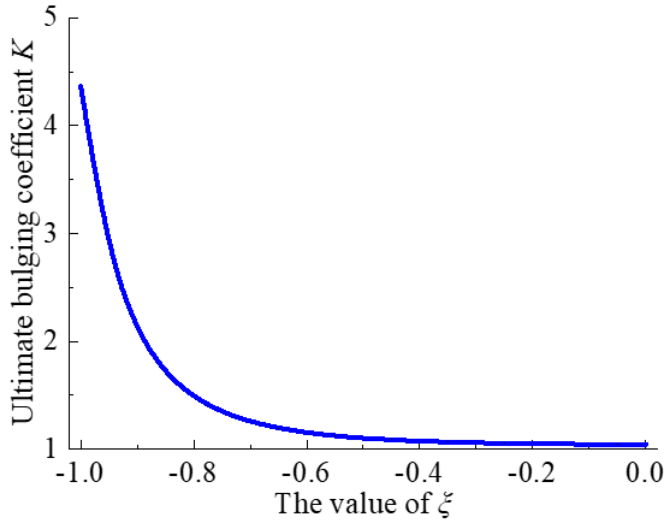

Figure 4. Effect of $\varepsilon_\rho/\varepsilon_\theta$ on the limit expansion forming coefficient

5 Numerical Simulation of Composite Mechanical Expansion Forming for Drive Axle Housing

Figure 5 shows a schematic diagram of the bridge arch section of a 5t commercial vehicle drive axle housing, with a minimum wall thickness of 8 mm, and the cross-section of the straight arm section of the bridge arch being a square with a side length of 100 mm. Using the proposed process, the pre-expanded tube billet is taken as the initial end, and a finite element simulation is carried out using the DEFORM-3D software to simulate the expansion process of the bridge arch of the 5t commercial vehicle drive axle housing made from seamless square tubes at room temperature.

Since the drive axle housing has axisymmetric shape characteristics, to improve computational efficiency, a 1/2 model of the bridge housing is used for the simulation. The tube billet material is medium-strength alloy structural steel 20Mn2, with a cross-sectional size specification of 100×100×8 mm. The area of a single cross-section at the maximum expansion position is about 1001 mm^2. According to the shape and size of the bridge housing, the area of the designed expansion mandrel surface is approximately 17966 mm^2. The radial motion rate of the expansion mandrel is 14.5 mm/s, and the friction coefficient between the mold and the tube billet is 0.12. The temperature of the tube billet is room temperature, and the convective heat transfer coefficient is 0.02 $\mathrm{N}\cdot(\mathrm{s}\cdot\mathrm{mm}\cdot{}^\circ\mathrm{C})^{-1}$, with a heat transfer coefficient between the billet and the mold of 5. The numerical simulation model of the drive axle housing bridge arch formation is shown in Figure 6. Figure 6 below gives a numerical simulation model of drive axle housing bridge arch formation.

To facilitate comparison of the effect of axial auxiliary thrust on the forming results, simulations were performed

for both cases: one with no axial auxiliary thrust and one with auxiliary thrust applied after pre-expansion. If the applied thrust on the driving expansion mandrel is 41 tons and the lateral auxiliary thrust is 112 tons, using the limit expansion forming theory derived in this paper, the limit expansion forming coefficient of the square tube under these conditions is approximately 1.983. Taking 90% of this value, the forming coefficient during composite mechanical expansion is 1.785. After pre-expansion, the maximum radial dimension of the bridge housing is 170 mm. The expansion coefficient of 1.785 theoretically allows the expansion mandrel to complete the bridge arch expansion in one secondary expansion.

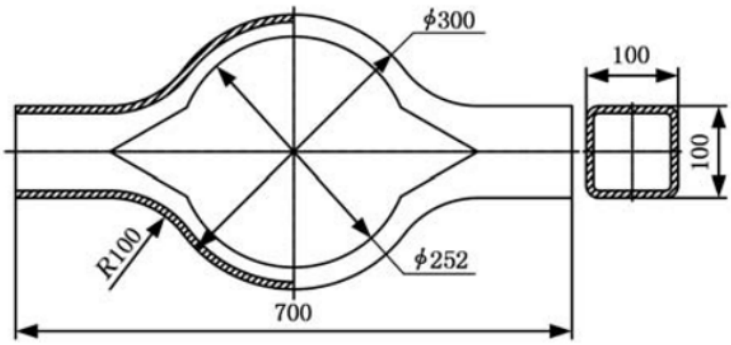

Figure 5. Schematic diagram of the drive axle housing bridge arch section

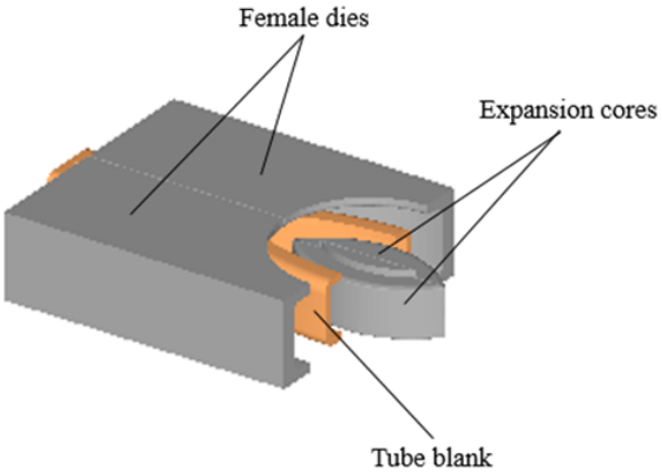

Figure 6. Finite element model of drive axle housing bridge arch forming

The stress and strain distribution in the bridge arch section of the drive axle housing under both conditions is shown in Figure 7 and Figure 8. During the radial expansion of the bridge arch, the equivalent stress and equivalent strain are most concentrated at the location where the preformed hole's two sides meet the straight arm section, where bending occurs (hereafter referred to as the crack-prone region). The reason for this is: at the beginning of the expansion, the expansion mandrel first contacts the inner wall of the expansion zone and forces it to move radially under the action of compressive stress, which also causes the opening angle at the preformed hole's end to enlarge. Therefore, the equivalent stress is mainly concentrated at the contact point between the expansion zone and the expansion mandrel, as well as at the corner of the preformed hole at both ends. In the mid- to late stages of the expansion process, the working surface of the expansion mandrel has fully adhered to the inner wall of the expansion zone, and the equivalent stress gradually merges and spreads throughout the entire expansion zone. As the opening angle at the preformed hole's end further enlarges, the equivalent stress becomes more concentrated at the corners of the preformed hole. During the forming process, the deformation mainly occurs at the corners of the preformed hole at both ends. As the expansion forming continues, the protrusions used for shaping on the expansion mandrel start to act on the inner edge of the preformed hole, leading to gradually increasing deformation at the region restricted by the protrusion on the inner edge. The top and side corners of the preformed hole, acting as stress concentration points,

cause the adjacent metal to flow toward these two areas, which results in the metal in other parts of the expansion zone being stretched, while the inner corners of the preformed hole remain in a tensile stress state, causing the wall thickness in this region to decrease. When there is no axial auxiliary thrust, the maximum equivalent stress in the crack-prone region is 795 MPa, which exceeds the tensile strength of 20Mn2 material at room temperature (785 MPa), and it is theoretically determined that tearing has occurred in this region. However, with 41 tons of axial auxiliary thrust, the maximum equivalent stress in the crack-prone region is 758 MPa, indicating that no rupture has occurred, showing the significant role of applying axial auxiliary thrust in ensuring the product quality of the bridge shell. Thus, axial auxiliary thrust becomes a key process parameter in the composite mechanical expansion process for the bridge arch.

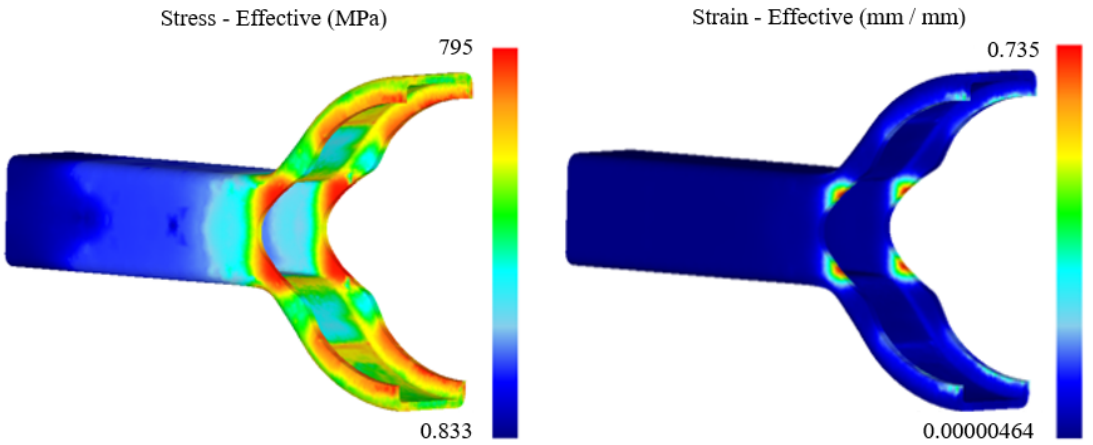

(a) Equivalent stress distribution (b) Equivalent strain distribution

Figure 7. Stress and strain distribution after expansion without axial thrust

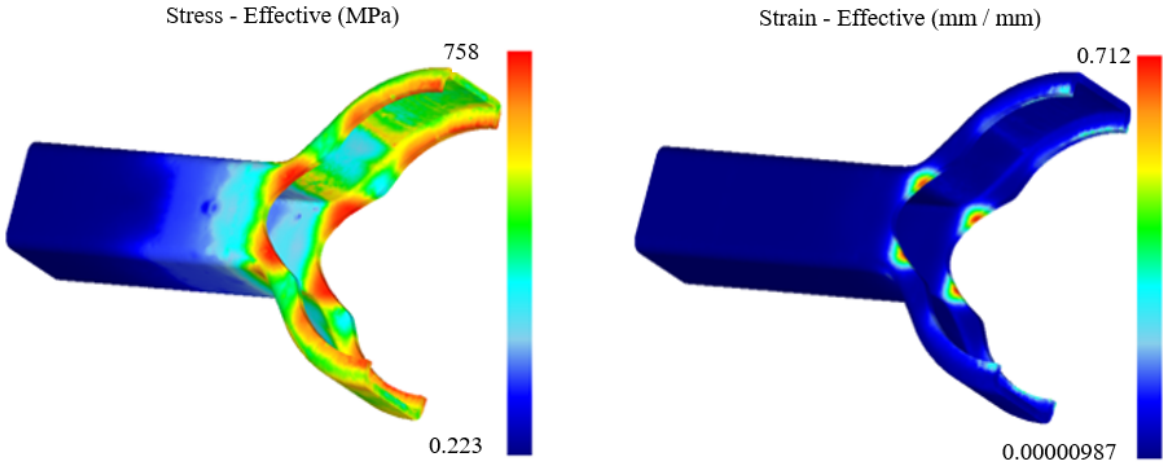

(a) Equivalent stress distribution (b) Equivalent strain distribution

Figure 8. Stress and strain distribution after expansion with axial thrust

In addition to checking whether the bending areas at both sides of the preformed hole have cracked, the reduction in wall thickness in the bridge arch expansion zone is also an important evaluation criterion for the shape quality of the drive axle housing. As shown in Figure 9, since the drive axle housing is symmetrically distributed, the 1/4 section of the bridge arch along the symmetry plane is taken for analysis. Starting from the top of the bridge arch after expansion, the wall thickness distribution along the cutting path a-b-c-d is studied to obtain the wall thickness reduction in the expansion zone at the end of the forming process. Under the condition of axial auxiliary thrust, the wall thickness distribution data along the a-b-c-d path of the bridge arch is shown in Table 1, and Figure 10

presents the corresponding trend of wall thickness distribution. The minimum wall thickness is 6.83 mm, and the wall thickness reduction rate is 14.6%. The specific location of this reduction is at approximately 147 mm along the a-b-c-d curve, i.e., at point E in Figure 10.

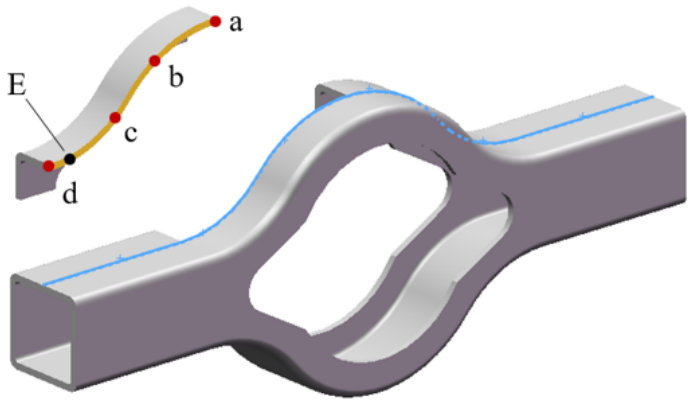

Figure 9. Schematic of bridge arch expansion zone cutting path

Table 1. Wall thickness distribution data along a-b-c-d path of the bridge arch (mm)

Arc Length	0	30	60	90	120	147	150	180	210
Wall Thickness	8.13	7.92	7.79	7.52	7.4	6.83	6.87	8.12	8

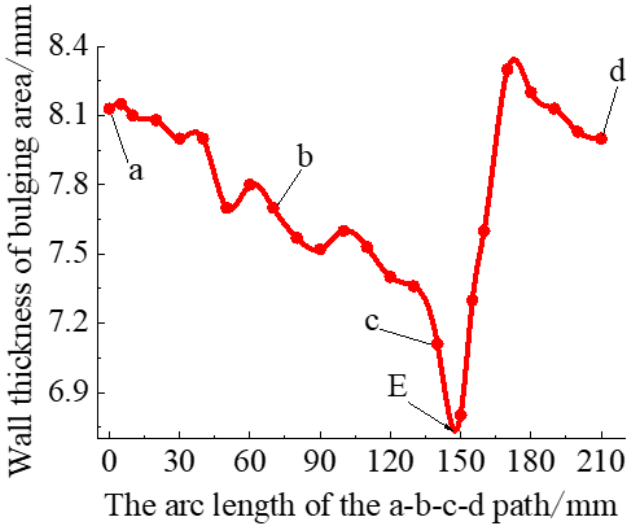

Figure 10. Wall thickness distribution in the bridge arch expansion zone

6 Key Parameter Determination and Orthogonal Experiment

Process parameters are crucial data in the manufacturing procedures of metal products. Researching and establishing reasonable process parameters is a necessary step in scientifically controlling the metal flow state, which is essential for effectively ensuring product forming quality [25–27]. At room temperature, the main process parameters involved in the composite mechanical expansion forming process of medium-sized commercial vehicle drive axle housings include: expansion mandrel movement speed v, axial auxiliary thrust T, and friction lubrication conditions μ. The friction in the production process involves the combined friction between the expansion mandrel and the inner wall of the steel tube, as well as between the outer wall of the steel tube and the inner wall of the die. During the expansion process, the contact area between the expansion mandrel and the die with the steel tube metal gradually

increases, and the confined forming space makes it difficult to apply lubrication repeatedly, causing the lubrication effect to be difficult to control precisely. Therefore, this paper focuses on the effects of expansion mandrel movement speed v and axial auxiliary thrust T on the wall thickness reduction degree η of the bridge arch and the wall thickness reduction degree β of the crack-prone region. Based on the tube blank specifications shown in Figure 5 and the limit expansion forming theory proposed in this paper, a 2-factor 5-level comprehensive simulation experimental plan was developed for these process parameters, as shown in Table 2. The simulation experiments were conducted based on the finite element model shown in Figure 6, and the results of the 25 experimental runs are shown in Table 3.

Table 2. Process parameter level table

Process Parameter	Level				
	1	2	3	4	5
Expansion Mandrel Speed $v/(\mathrm{mm/s})$	5	10	15	20	25
Axial Auxiliary Thrust $F/(t)$	30	35	40	45	50

Table 3. Simulation experiment plan and results

Experiment No.	Process Parameters		Results	
	Expansion Mandrel Speed v (mm/s)	Axial Auxiliary Thrust T (t)	Bridge Arch Wall Thickness Reduction Rate η (%)	Crack-Prone Region Wall Thickness Reduction Rate β (%)
1	5	30	16.48	31.81
2	5	35	15.11	31.38
3	5	40	14.71	31.37
4	5	45	13.71	31.04
5	5	50	13.05	31.45
6	10	30	16.14	31.46
7	10	35	14.94	31.82
8	10	40	14.20	31.78
9	10	45	13.51	31.50
10	10	50	11.23	31.47
11	15	30	15.93	31.61
12	15	35	14.85	31.93
13	15	40	13.85	32.03
14	15	45	13.31	32.08
15	15	50	10.05	32.15
16	20	30	15.69	32.25
17	20	35	14.71	32.25
18	20	40	13.69	32.31
19	20	45	12.85	32.32
20	20	50	9.79	32.31
21	25	30	15.30	32.18
22	25	35	13.90	32.66
23	25	40	13.48	32.67
24	25	45	12.64	32.67
25	25	50	7.04	32.69

7 Analysis of Orthogonal Experiment Results and Parameter Optimization

Based on the simulation experiment data shown in Table 3, multivariate regression fitting of the relationships between the process parameters and the wall thickness reduction rates of the bridge arch and crack-prone region was performed using the second-order response surface method in MATLAB software. The parameter estimation results and variance analysis results of the regression equation are shown in Table 4 and Table 5.

Based on the results of multivariate regression fitting, the regression equations for the bridge arch wall thickness reduction rate η and the crack-prone region wall thickness reduction rate β as functions of expansion mandrel speed v and axial auxiliary thrust T are shown in Eqs. (13) and (14), respectively.

$$\eta = 4.0968 + 0.2768v + 0.6941T - 0.0086vT - 0.0011v^2 - 0.0103T^2 \tag{13}$$

$$\beta = 31.0163 - 0.0277v + 0.0317T + 0.0019vT + 0.0004v^2 - 0.0007T^2 \tag{14}$$

Table 4. Bridge arch expansion zone wall thickness reduction rate regression equation parameter estimation and variance analysis results

Parameter Estimation			
Variable	Estimated Value	Standard Error	p
Constant Term	4.0968	5.5658	0.4784
v	0.2768	0.1549	0.0898
T	0.6941	0.2774	0.0216
νT	-0.0086	0.0029	0.0073
v^2	-0.0011	0.0034	0.7553
T^2	-0.0103	0.0034	0.0072

Variance Analysis				
Source	Degrees of Freedom	Sum of Squares	F-value	p-value
Regression	5	104.087	40.7505	$3e-9$
Residual	19	9.7007		
Total	24	113.7294		

Root Mean Square Error 0.7145; Determination Coefficient $R^2 = 0.9147$
Mean of Dependent Variable 13.6064; Adjusted Determination Coefficient ${R^2}_{adj} = 0.8923$

Table 5. Crack-prone region wall thickness reduction rate regression equation parameter estimation and variance analysis results

Parameter Estimation			
Variable	Estimated Value	Standard Error	p
Constant Term	31.0163	1.3681	0.0001
v	-0.0277	0.0374	0.4676
T	0.0317	0.0670	0.6419
νT	0.0019	0.0007	0.0140
v^2	0.0004	0.0008	0.5999
T^2	-0.0007	0.0008	0.4123

Variance Analysis				
Source	Degrees of Freedom	Sum of Squares	F -value	p-value
Regression	5	4.8013	32.2593	7e-9
Residual	19	0.5656		
Total	24	5.3669		

Root Mean Square Error 0.1725; Determination Coefficient $R^2 = 0.8946$
Mean of Dependent Variable 31.9676; Adjusted Determination Coefficient ${R^2}_{adj} = 0.866$

In this paper, the determination coefficient R^2 (or adjusted determination coefficient ${R^2}_{adj}$) is used to verify the accuracy of the regression Eqs. (13) and (14) in reflecting the relationship between the design variables and the objective function. That is, the closer the value of the determination coefficient R^2 (or adjusted determination coefficient ${R^2}_{adj}$) is to 1 , the higher the fitting accuracy of the regression equation. When the p-value of the F-test for variance is less than 0.05, the linear relationship of the equation is considered significant. If the ppp-value is less than 0.01, the linear relationship is considered highly significant. As shown in Table 3, with $R^2 = 0.9147$ and ${R^2}_{adj} = 0.8923$, both values are close to 1, and $P = 3e-9 < 0.01$, indicating that the linear relationship of regression Eq. (13) is highly significant with high fitting accuracy. Similarly, in Table 5, with $R^2 = 0.8946$ and ${R^2}_{adj} = 0.8669$, both values are also close to 1, and $P = 7e-9 < 0.01$, confirming that the linear relationship of regression Eq. (14) is highly significant with high fitting accuracy. Therefore, the constructed response surface equations have high predictive accuracy and can well reflect the response relationship between influencing factors and the objective function.

From the parameter estimation data in Table 4, the p-value corresponding to the expansion mandrel speed v is $0.0898 > 0.05$, indicating that the effect of v on the bridge arch wall thickness reduction rate η is not significant. In Table 4, the p value corresponding to v is $0.4676 > 0.05$, indicating that v also does not significantly affect the crack-prone region wall thickness reduction rate β. In Table 4, the p-value corresponding to axial auxiliary thrust T is $0.0216 < 0.05$, indicating that axial auxiliary thrust T has a significant effect on the bridge arch wall thickness reduction rate η. However, in Table 5, the p-value corresponding to axial auxiliary thrust T is $0.6419 > 0.05$, suggesting that when the thrust is sufficiently large, T does not significantly affect the crack-prone region wall thickness reduction rate β. Using Origin software, response surface plots of the bridge arch wall thickness reduction rate η and crack-prone region wall thickness reduction rate β as functions of expansion mandrel speed v and axial auxiliary thrust T were plotted, as shown in Figure 11 and Figure 12. From Figure 11, it can be seen that the bridge

arch wall thickness reduction rate decreases with increasing expansion mandrel speed and axial auxiliary thrust. Figure 12 shows that the crack-prone region wall thickness reduction rate β increases with increasing expansion mandrel speed and axial auxiliary thrust.

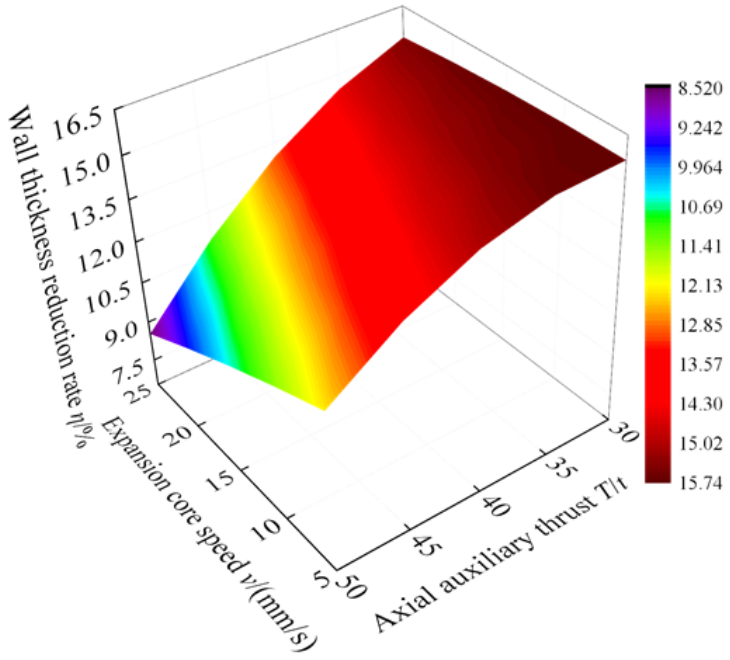

Figure 11. Response surface of bridge arch wall thickness reduction rate as a function of expansion mandrel speed and axial auxiliary thrust

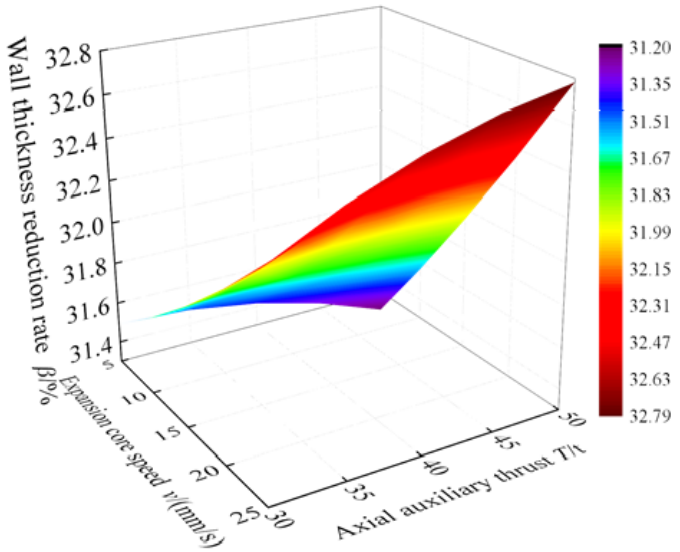

Figure 12. Response surface of crack-prone region wall thickness reduction rate as a function of expansion mandrel speed and axial auxiliary thrust

After the composite mechanical expansion, the smaller the wall thickness reduction rate η of the bridge arch expansion zone and the smaller the wall thickness reduction rate β of the crack-prone region, the higher the forming quality of the bridge shell. Therefore, the optimal evaluation criterion is the simultaneous minimum value of the wall thickness reduction rate and the crack-prone region wall thickness reduction rate. Based on the response surface model derived, the process parameters of the bridge arch composite mechanical expansion were optimized. This paper uses Design-Expert software to solve the response surface model and obtain the expected values of the model

under different combinations of process parameters. The higher the expected value corresponding to a parameter combination, the better the predicted forming effect. According to the predicted expected values from largest to smallest, the top 5 parameter combinations are listed in Table 6.

Table 6. Optimized parameter combinations

No.	$v/(\mathrm{mm/s})$	T/t	$\eta/\%$	$\beta/\%$	Expected Value
1	18.2709	47.216	10.811	31.382	0.827
2	19.0865	46.3546	11.08	31.386	0.813
3	17.5817	46.8497	11.517	31.398	0.806
4	20.3091	46.0782	11.629	31.405	0.798
5	15.2197	44.0292	11.832	31.412	0.792

In combination with actual engineering, the process parameters with the highest expected value in Table 6 were rounded to integers, resulting in an expansion mandrel speed of 18 mm/s and an axial auxiliary thrust of 47 t. Using this rounded optimized parameter combination, numerical simulation was conducted again with the finite element model for the drive axle bridge arch forming, as shown in Figure 6. The minimum wall thickness in the bridge arch expansion zone was measured as 7.133 mm with a reduction rate of 10.832%, and the minimum wall thickness in the crack-prone region was 5.489 mm with a reduction rate of 31.389%. The simulation results were basically consistent with the optimized predicted results. The small numerical differences between the results were mainly due to parameter rounding and the uneven node distribution caused by the model meshing process, which led to slight differences in wall thickness measurements. Comparing with the original experimental data, the optimized parameters after rounding are within the experimental parameter range and have advantages in suppressing wall thickness reduction compared to other parameters of the same level, reflecting the effectiveness of the optimization.

8 Experimental Verification

To verify the feasibility and parameter optimization effect of the proposed composite mechanical expansion process for the drive rear axle housing, a corresponding composite mechanical expansion mold and braking mechanism were designed, and experiments were conducted on a 1000kN/4000kN×2 multi-directional hydraulic press, as shown in Figure 5, for a 5-ton commercial vehicle drive rear axle housing. The material, specifications, and forming parameters of the seamless steel pipe were identical to those used in the numerical simulation. It is important to emphasize that during the radial expansion forming experiment, the movement of the expansion mandrel was driven by the braking wedge, and the rear side of the expansion mandrel had grooves to act as a guide rail to limit the movement of the braking wedge. In the experiment, the steel pipe with pre-made holes was first fixed in the mold. The hydraulic press slider was driven to push the pre-expansion wedge blind through the pre-made hole to form space for the expansion mandrel on both sides of the bridge arch. Then, the composite mechanical expansion experiment began, with the hydraulic press slider driving the braking wedge downward, causing the two expansion mandrels to move in reverse. When the expansion mandrels contacted the inner wall of the expansion zone, the oil cylinders on both sides of the hydraulic press applied axial auxiliary thrust to the two ends of the steel pipe until the expansion was complete. The experimental tooling is shown in Figure 13.

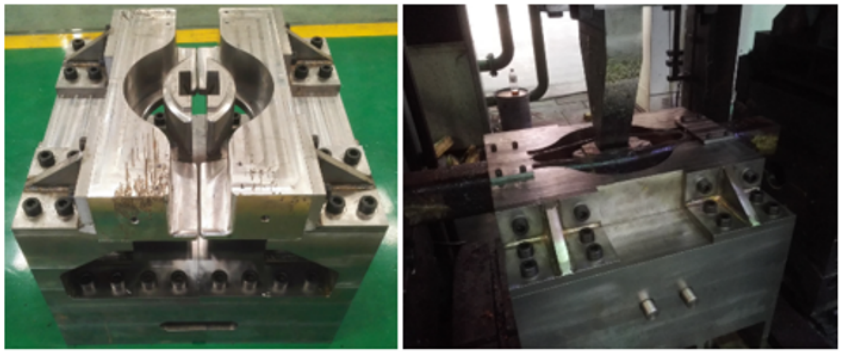

(a) Forming test tooling (b) Forming test process

Figure 13. Experimental tooling and forming process

As shown in Figure 14, after performing radial mechanical expansion without applying axial auxiliary thrust, cracks appeared at the areas where the expansion zone connected with the straight arm section, consistent with the

numerical simulation results. Using the optimized process parameter combination, the formed drive rear axle housing specimen is shown in Figure 15. The forming effect of the specimen was good, and no tearing occurred in the crack-prone region, fully demonstrating the necessity of applying axial auxiliary loads to prevent tearing defects.

Figure 14. Cracking of the bridge shell and cracks

(a) Post-test drive rear axle shell

(b) Wall thickness reduction in the fragile zone

Figure 15. Bridge shell specimen and wall thickness reduction in the fragile zone

Table 7. Wall thickness distribution and error along path a-b-c-d of the bridge arch

Arc Length /mm	Simulated Wall Thickness /mm	Measured Wall Thickness /mm	Error /mm
0	8.098	8.131	0.033
30	7.988	8.025	0.037
60	7.852	7.828	0.024
90	7.611	7.523	0.088
120	7.475	7.406	0.069
150	7.133	7.115	0.018
180	8.153	8.204	0.051
210	8	8	0

As mentioned earlier, a laser thickness gauge was used to measure the wall thickness distribution of the bridge arch expansion zone along the 1/4 arc segment. The measured wall thickness distribution was compared with the simulation results obtained using the optimized process parameters, as shown in Table 7. The measured minimum wall thickness was 7.115 mm, with a thinning rate of 11.057%. Figure 16 shows the corresponding specific wall thickness distribution trends. In addition, the measured minimum wall thickness in the fragile zone was 5.487 mm, with a thinning rate of 31.412%.

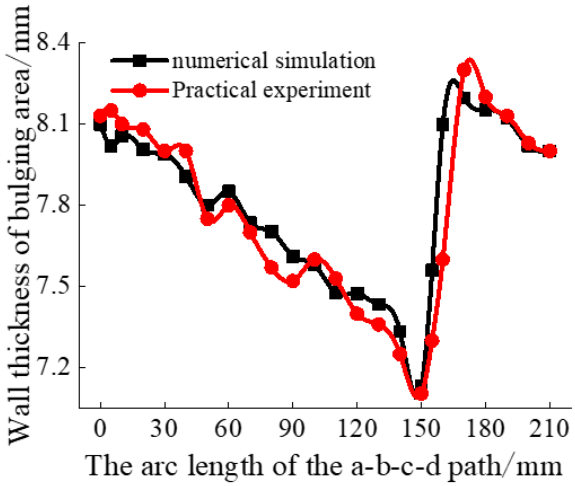

Figure 16. Comparison of measured wall thickness with numerical simulation wall thickness distribution in the bridge arch expansion zone

As shown in Figure 16, the continuous change in the internal wall's compressive stress state during the expansion process causes the wall thickness to gradually decrease, with some slight fluctuations. The process emphasized here is a radial expansion process driven mainly by the expansion core's motion, where the top of the arc face of the expansion core is in contact with the inner wall of the expansion zone. This causes the top of the inner wall of the bridge arch expansion zone to be subjected to greater compressive stress from the expansion core. Therefore, the top and side ends of the bridge arch expansion zone, where it connects with the straight arm section, are regions of relatively concentrated stress during the forming process. This leads to the adjacent metal flowing toward these two areas, thereby stretching the metal in other parts of the expansion zone. As the expansion process continues, the bending tendency at the junction of the bridge arch and the straight arm section on both sides increases. The particles in the bending region experience mutual extrusion to a certain extent, forming a thickening effect, which results in less thinning in the last part of the bending region. The areas where the inner wall of the expansion zone gradually contacts the expansion core are subject to compressive stress, so the thinning tendency gradually decreases. On the other hand, areas that have never contacted the expansion core and are not influenced by bending deformation experience the greatest stretching. From Figure 16, it can be observed that the wall thickness of the inner wall of the expansion zone that is in contact with the expansion core decreases approximately linearly from the top toward the side, while the wall thickness gradient increases sharply where it departs from the expansion core. The wall thickness increases significantly after the thinnest point and returns to its original value. In this experiment, the thinnest wall thickness occurs at about 150 mm along the arc length of the a-b-c-d path starting at point a in Figure 9. Point E is located at the critical region affected by the thickening effect due to bending deformation, where the thinning due to stretching is most pronounced. In addition, Figure 16 shows that the experimental wall thickness distribution closely matches the numerical simulation. The experimental results verify the feasibility of the proposed drive rear axle shell composite mechanical expansion forming process and the importance of axial auxiliary loads in improving the stress state of the expansion zone and preventing tensile fracture defects. Additionally, the results reflect the rationality of the process parameters, demonstrating that the optimized process data can serve as a reference for actual debugging. This has significant guiding value for the parameter control in the precision plastic forming process of commercial vehicle drive rear axle shells.

9 Conclusions

(1) This paper proposes a new composite mechanical expansion forming process suitable for medium-sized commercial vehicle drive rear axle shells. The core process of this technology is to apply axial loads to both ends of seamless steel pipes during radial mechanical expansion.

(2) The expression for the composite mechanical expansion coefficient of seamless steel pipe billets in the deformation zone under sub-recrystallization temperature conditions is derived. It reveals the relationship between the limit expansion forming coefficient and force matching in the expansion zone under the condition that the metal is not torn. The range of axial auxiliary loads during radial expansion is provided, where the absolute value of compressive stress generated by the auxiliary thrust at the vertical section of the maximum expansion area of the bridge arch shall not exceed the real yield stress of the metal material at that temperature.

(3) Under the premise of expansion driven mainly by the expansion core, axial auxiliary thrust does not alter the metal flow trend in the expansion zone, but it effectively alleviates stress concentration. The application of axial auxiliary loads is necessary to prevent tensile fracture defects during the radial expansion process.

(4) Based on orthogonal simulation experimental design, the multi-objective optimization of the response surface is conducted to minimize the thinning rate of the bridge arch expansion zone and the fragile zone. The results show that the thinning rate of the bridge arch expansion zone decreases with an increase in the expansion core's movement speed and axial auxiliary thrust, while the thinning rate of the fragile zone increases. However, the movement speed of the expansion core has little effect on both the bridge arch expansion zone and the fragile zone's thinning rates. Axial auxiliary thrust significantly influences the thinning rate of the bridge arch expansion zone, but its effect on the thinning rate of the fragile zone is negligible when sufficiently large.

(5) The multi-objective optimization model was solved, and the process parameters obtained for the site conditions were: expansion core movement speed of 18 mm/s and axial auxiliary thrust of 47 t. Numerical simulations and process experiments were conducted using the optimized process parameters for the 5t commercial vehicle drive rear axle shell. The measured results for wall thickness reduction in the bridge arch expansion zone and the fragile zone closely matched, while expansion without axial auxiliary thrust caused cracking. This validates the feasibility of the proposed drive rear axle shell composite mechanical expansion forming process and the optimization of the process parameters.

In conclusion, this paper innovatively proposes a new composite mechanical expansion forming process for medium-sized commercial vehicle drive rear axle shells, revealing the relationship between the expansion coefficient and force matching through theoretical derivation. Multi-objective optimization was employed to reduce the thinning rate in the expansion zone, and the feasibility of the process and optimization of the process parameters were experimentally validated. This study can promote the shift of the commercial vehicle drive rear axle shell production model from decentralized assembly to overall manufacturing, improving production efficiency and quality. It also provides new ideas for the development of supporting production equipment through the integration of smart and automated technologies and offers valuable references for future research on deep exploration of component performance and fine-tuning of process parameters.

Funding

This research was funded by the Youth Fund Project for Scientific Research of Higher Education Institutions in Hebei Province (Grant No.: QN2025015); the 14th Five Year Plan Project for Higher Education Science Research of Hebei Higher Education Association (Grant No.: GJXHZ2024-30); and Self Funded Project of Langfang Science and Technology Plan (Grant No.: 2024011078).

Data Availability

The data used to support the research findings are available from the corresponding author upon request.

Conflicts of Interest

The authors declare no conflict of interest.

References

[1] M. U. Yousaf, T. Aized, A. Shabbir, M. Ahmad, and H. Z. Nabi, "Automobile rear axle housing design and production process improvement using Failure Mode and Effects Analysis (FMEA)," *Eng. Fail. Anal.*, vol. 154, p. 107649, 2023. https://doi.org/10.1016/j.engfailanal.2023.107649

[2] X. D. Wang, L. D. Wang, M. Jin, H. Liu, and N. Wu, "Mechanism analysis and engineering experiment of multi-directional pressing-forming complex large-size automobile axle housing," *Int. J. Adv. Manuf. Technol.*, vol. 120, pp. 1295–1314, 2022. https://doi.org/10.1007/s00170-022-08845-6

[3] C. Mi, Y. Li, C. Zhang, D. Zhang, X. Liu, X. Hu, and D. Zhang, "An energy-based anti-fatigue optimization design method of welded rear axle housing in a mining dump truck," *Mechanika*, vol. 29, no. 4, pp. 317–323, 2023. https://doi.org/10.5755/j02.mech.32371

[4] F. Zhao, "Finite-element analysis on lightweight material of drive axle housing," *Rev. Compos. Mater. Av.*, vol. 31, no. 1, pp. 41–49, 2021. https://doi.org/10.18280/rcma.310106

[5] M. Prabhakar, A. Prasad, and M. Paswan, "Realistic correlation of damage estimate in axle housing of commercial vehicles using road load data with bench testing results and failure analysis to overcome hot forming losses," *SAE Int. J. Commer. Veh.*, vol. 14, no. 1, pp. 3–21, 2021. https://doi.org/10.4271/02-14-01-0001

[6] G. S. Kumar and L. A. Kumaraswamidhas, "Design optimization focused on failures during developmental testing of the fabricated rear-axle housing," *Eng. Fail. Anal.*, vol. 120, p. 104999, 2021. https://doi.org/10.1016/j.engfailanal.2020.104999

[7] M. Prabhakar, A. K. Prasad, and M. K. Paswan, "Influence of loading sequence and residual stresses affecting the fatigue life of axle housing and crack path analysis using local approaches," *Eng. Fail. Anal.*, vol. 116, p. 104753, 2020. https://doi.org/10.1016/j.engfailanal.2020.104753

[8] M. Prabhakar, A. K. Prasad, M. K. Paswan, and V. Tendulkar, "Fatigue life prediction of welding in axle housing using notch stress approach," *Mater. Today Proc.*, vol. 22, pp. 2233–2240, 2020. https://doi.org/10.1016/j.matpr.2020.03.304

[9] G. S. Kumar and L. A. Kumaraswamidhas, "Design optimization focused on failures during developmental testing of the fabricated rear-axle housing," *Eng. Fail. Anal.*, vol. 120, p. 104999, 2021. https://doi.org/10.1016/j.engfailanal.2020.104999

[10] Y. J. Sun, Y. Guo, X. Li, and S. Wang, "Optimization of the bridge shell structure of the mining dump truck-driven axle," *J. Liaoning Tech. Univ.-Nat. Sci.*, vol. 41, no. 4, pp. 350–354, 2022. https://doi.org/10.11956/j.issn.1008-0562.2022.04.010

[11] M. Prabhakar, A. Prasad, and M. Paswan, "Realistic correlation of damage estimate in axle housing of commercial vehicles using road load data with bench testing results and failure analysis to overcome hot forming losses," *Commer. Veh.*, vol. 14, no. 1, pp. 3–21, 2021. https://doi.org/10.4271/02-14-01-0001

[12] M. Prabhakar, A. K. Prasad, and M. K. Paswan, "Influence of loading sequence and residual stresses affecting the fatigue life of axle housing and crack path analysis using local approaches," *Eng. Fail. Anal.*, vol. 116, p. 104753, 2020. https://doi.org/10.1016/j.engfailanal.2020.104753

[13] C. K. Wen, Z. Y. Liu, G. W. Wu, C. J. Zhao, L. P. Chen, Y. X. Yin, and Z. J. Meng, "Digital twin-driven fatigue life prediction framework of mechanical structures using a power density theory: Application to off-road vehicle front axle housing," *Meas.*, vol. 220, p. 113352, 2023. https://doi.org/10.1016/j.measurement.2023.113352

[14] B. Zheng, S. Y. Fu, and J. L. Lei, "Topology optimization and multiobjective optimization for drive axle housing of a rear axle drive truck," *Mater.*, vol. 15, no. 15, p. 5268, 2022. https://doi.org/10.3390/ma15155268

[15] S. Maity, V. Gulhane, and P. Sondar, "Mitigation of friction weld failure due to oxides in automobile axle housing," *J. Fail. Anal. Prev.*, vol. 24, pp. 1–15, 2024. https://doi.org/10.1007/s11668-024-02064-9

[16] J. Y. Song, H. D. Pan, W. T. An, and J. Y. Sun, "Strength and life analysis of a heavy truck axle housing," *Int. J. Automot. Technol.*, pp. 1–7, 2024. https://doi.org/10.1007/s12239-024-00165-w

[17] B. F. Zhang, Z. Zhao, Y. X. Li, X. H. Zhang, X. J. Li, D. N. Hao, and Z. T. Zhang, "Design and analysis of a piezoelectric energy harvesting shock absorber for light truck applications," *Appl. Energy*, vol. 377, p. 124569, 2025. https://doi.org/10.1016/j.apenergy.2024.124569

[18] Z. C. Wang, "Statics analysis and fatigue life study of integral cold expansion forming drive axle housing considering residual stress," Ph.D. dissertation, Anhui University of Technology, Maanshan, China, 2022.

[19] J. C. Yang, L. Z. Wang, and C. G. Dai, "Optimization and experimental study on the process parameters of high pressure forming for axle housing," *J. Mech. Strength*, vol. 43, no. 3, pp. 747–751, 2021.

[20] L. Pan, "Research on forming process and key technologies for manufacturing integral driving axle housing of commercial vehicle," Ph.D. dissertation, China Academy of Machinery Science and Technology, Beijing, China, 2017.

[21] Y. Zong, "Research on mechanical thermal expansion forming technology of integral drive axle housing," Ph.D. dissertation, Jilin University, Changchun, China, 2021.

[22] Y. Wang, "Research on integral mechanical thermal expansion forming process of heavy duty vehicle rear axle housing," Ph.D. dissertation, Jilin University, Changchun, China, 2014.

[23] N. Golovina, "The stress-strain curve model in the form of an extremal of a non-integrable linear variation form," *Ind. Lab. Diagn. Mater.*, vol. 89, no. 3, pp. 80–88, 2023. http://doi.org/10.26896/1028-6861-2023-89-3-80-86

[24] Y. Hui, J. J. Wu, M. Z. Wang, X. P. Zhan, and H. Fan, "Equivalent strain hardening exponent of anisotropic materials based on spherical indentation response," *Trans. Nonferrous Met. Soc. China*, vol. 29, no. 1, pp. 77–87, 2019. https://doi.org/10.1016/S1003-6326(18)64917-9

[25] Y. Liu, H. Gu, Z. Leng, C. Peng, Z. Wang, and S. Zhang, "Study on the optimization of process parameters for submerged arc welding of hydrogen production reactor material," *Coatings*, vol. 14, no. 12, p. 1548, 2024. https://doi.org/10.3390/coatings14121548

[26] C. Shu, Z. Y. Zheng, P. R. Lei, H. J. Xu, X. D. Shu, and K. Essa, "Optimization of process parameters for TC11 alloy via tailoring scanning strategy in laser powder bed fusion," *Front. Mater. Sci.*, vol. 18, no. 4, p. 240710, 2024. https://doi.org/10.1007/s11706-024-0710-z

[27] N. Senthilkumar, K. Sabari, P. Azhagiri, and M. Yuvaperiyasamy, "Impact of tool geometry and friction stir welding parameters on AZ31 magnesium alloy weldment wear behaviour and process optimization," *Weld. Int.*, vol. 38, no. 12, pp. 805–822, 2024. https://doi.org/10.1080/09507116.2024.2430208